Temporal and Spatial Dynamics of Hepatic Stellate Cell Activation in Intrahepatic Cholangiocarcinoma

Short Title: Hepatic Stellate Cell in Cholangiocarcinoma

Cheng Tian[1*], **Liyuan Li**[1*], Qingfei Pan[2], Yizhen Li[1], Wentao Yang[2], Li Fan[1], Anthony Brown[1], Michelle Morrison[3], Kaushik K. Dey[1], Eric J. Norris[4], Jun J. Yang[1], Jiyang Yu[2], Evan S. Glazer[3], and Liqin Zhu[1]

[1]Department of Pharmacy and Pharmaceutical Sciences, St. Jude Children's Research Hospital, Memphis, Tennessee, United States

[2]Department of Computational Biology, St. Jude Children's Research Hospital, Memphis, Tennessee, United States

[3]Departments of Surgery and Cancer Center, College of Medicine, The University of Tennessee Health Science Center, Memphis, Tennessee, United States

[4]STEMCELL Technologies, Brentwood, Tennessee, United States

[*] **Equal contribution**

Correspondence

Liqin Zhu, PhD, Department of Pharmacy and Pharmaceutical Sciences, St. Jude Children's Research Hospital, 262 Danny Thomas Place, Memphis, Tennessee 38105-3678. E-mail: liqin.zhu@stjude.org; fax: (901) 595-8869; tel: (901) 595-5250.

Keywords

Intrahepatic cholangiocarcinoma, intratumoral and peritumoral hepatic stellate cells, Vcam1

Abbreviations

ICC	Intrahepatic cholangiocarcinoma
ECC	extrahepatic cholangiocarcinoma
HCC	Hepatocellular carcinoma
HSC	Hepatic stellate cells
A-HSC	activated HSC
itHSC	Intratumoral HSC
ptHSC	Peritumoral HSC
pTME	Peritumoral microenvironment
HC	Hepatocyte
WLC	Whole liver cell
CAF	Cancer-associated fibroblast
DTC	Disseminated tumor cells
PPTR	$Prom1^{CreERT2}$; $Pten^{flx/flx}$; $Tp53^{flx/flx}$; Rosa-ZsGreen
mTmG	$B6.129(Cg)\text{-}Gt(ROSA)26Sor^{tm4(ACTB\text{-}tdTomato,\text{-}EGFP)Luo}/J$
ZsG	Rosa-ZsGreen
TdT	Rosa-tdTomato
RFP	Red Fluorescent Protein
GFP	Green Fluorescent Protein
AW400	AggreWell 400
CM	Conditioned Media
TVI	Tail Vein Injection
IHC	Immunohistochemistry
GSEA	Gene set enrichment analysis

Grant Support: This work was supported by American Cancer Society Research Scholar Grant RSG-18-026-01.

Disclosures: None.

Author Contributions: C.T. and L.L. conducted most of the biological experiments. Q.P. and W.Y. conducted the bioinformatic analyses. Y.L., L.F., and A.B. conducted experiments. M.M, K.K.D, E.N., J. J. Y., J. Y., and E.S.G. provided technical and intellectual support. L.Z. conceived and oversaw the research. All authors contributed to the writing of the manuscript.

Transcript Profiling: To be submitted.

Data Sharing Statement: Data, analytic methods, and study materials will be made available to other researchers upon request.

ABSTRACT

Background and Aims

Intrahepatic cholangiocarcinoma (ICC) is characterized by its highly desmoplastic stroma mainly composed of myofibroblasts derived from activated hepatic stellate cells (HSCs). The role of HSCs in ICC development remains controversial. We aim to dissect the function of HSCs in ICC development.

Methods

An orthotopic allograft of metastatic ICC was generated to track the activation of intra- and peri-tumoral HSCs (itHSCs and ptHSCs, respectively). Multiple coculture systems were established to assess the impact of itHSCs and ptHSCs on ICC development. RNA-seq transcriptomic profiling was performed to examine ICC-induced liver host response.

Results

Activated itHSCs and ptHSCs are found in ICC patient tumors and surrounding liver. Tracking HSC in the ICC allograft model reveals HSC activation starting at the tumor border and extending into both tumor core and peritumoral liver when tumor progresses. In vitro coculture assays identify a surprising suppressive effect of ptHSCs on ICC cell growth in contrast to the pro-proliferative effect of itHSCs. Prolonged ICC-ptHSC interaction elicits tumor cell dissemination in vitro. ICC dissemination in vivo temporally and spatially coincides with further HSC activation in the liver which shows a protective effect on tumor-induced hepatocyte death. ICC-ptHSC interaction induces Vcam1 upregulation in the tumor cells which fine tunes the balance between ICC growth and dissemination. Transcriptomic analysis of the ICC allograft model reveals broad peritumoral changes in liver metabolism, oncogenic activation, and immune response.

Conclusion

In this study, we demonstrate that HSCs are activated during ICC development in a temporal- and spatial-specific manner and play a dynamic role in the intricate ICC-liver interaction.

INTRODUCTION

Cholangiocarcinoma is the second most common hepatic tumor after hepatocellular carcinoma (HCC). It is believed to originate from the biliary tracts within or outside the liver which lead to the development of intrahepatic or extrahepatic cholangiocarcinoma (ICC or ECC, respectively). ICC has a worse prognosis than ECC and is one of the deadliest cancers overall.[1, 2] Approximately one-third of ICC patients present with metastases at the diagnosis and up to two-third of patients experience and eventually succumb to relapse. Modern therapy has been designed based on ICC tumor biology but only marginally increased patient overall survival thus far.[3, 4]

One of the most prominent characteristics of ICC is its highly desmoplastic stroma. This has led to investigations on cancer-associated fibroblasts (CAFs) as well as hepatic stellate cells (HSCs), the major source of liver myofibroblasts,[5] in ICC progression.[6-10] Findings from these studies remain inconsistent on whether the fibrotic components function to promote or restrain ICC progression. One of the potential reasons accounting for this inconsistency is that these studies did not differentiate the fibrous components regarding their temporal and spatial relationship to ICC development. The liver is one of the few internal organs that are developmental equipped with a complex damage-response machinery to protect its vital function in metabolism.[11, 12] Considering that nearly every chronic liver condition eventually results in liver fibrosis,[13] it is conceivable that a growing malignant mass will elicit various fibrotic responses in the liver during its progression, resulting in a dynamic tumor-liver interaction that dictates tumorigenesis. Indeed, recent studies on HCC patients, although limited, have revealed the presence of activated HSCs (A-HSCs) and myofibroblasts in the peritumoral liver that are associated with metastasis and recurrence.[14, 15] We reason that investigating the spatial and temporal activation of HSCs elicited by ICC development will serve as one of the first efforts to map the host response to this rare but deadly cancer, providing new insights into understanding its aggressive clinical behaviors. To do so, we acquired a cohort of ICC patient tumors resected without neoadjuvant treatment and examined HSC activation in the tumor as well as the tumor-surrounding liver. We then tracked HSC activation in the tumor and liver in an orthotopic

allograft model of metastatic ICC we established in the laboratory. To specifically assess the impact of intra- and peri-tumoral HSCs (referred to as itHSCs and ptHSCs hereafter) on ICC progression, we developed multiple novel coculture systems to model tumor-liver interaction with a particular focus on ptHSCs. Lastly, we performed an RNAseq-based transcriptomic comparison of the liver tissues collected from normal and ICC-bearing mice to examine the broad peritumoral changes elicited by ICC development.

METHODS

Clinical Samples

The ICC patient tumor samples were obtained under a protocol approved by the Institutional Review Boards at both St. Jude Children's Research Hospital and The University of Tennessee Health Science Center.

Mice

Two-month-old male and female *B6.129(Cg)-Gt(ROSA)26Sor*$^{tm4(ACTB-tdTomato,-EGFP)Luo}$*/J* (*mTmG*) mice (Stock No. 007576, Jackson Laboratory, Bar Harbor, ME, USA) were used for primary cell isolation from the liver. Two-month-old male and female *Crl:CD1-Foxn1*$^{nu/nu}$ (CD-1 nude) mice (Strain Code 086, Charles River, Wilmington, MA, USA) were used for ICC orthotopic transplantation and tail vein injection. Animal protocols were approved by the St. Jude Animal Care and Use Committee. All mice were maintained in the Animal Resource Center at St. Jude Children's Research Hospital (St. Jude). Mice were housed in ventilated, temperature- and humidity-controlled cages under a12-hr light/12-hr dark cycle and given a standard diet and water *ad libitum*.

Cell Culture

Two ICC tumor cell lines, PPTR-1 and -2, were established from *Prom1*^{CreERT2}*; Pten*$^{flx/flx}$*; Tp53*$^{flx/flx}$*; Rosa-ZsGreen* (PPTR) liver cancer organoids[16] and maintained in DMEM (Corning Inc, Corning, NY, USA) supplemented with 10% fetal bovine serum (FBS) and antibotics. Primary mouse HSCs were purchased (Cat No. M5300-57, ScienCell Research Laboratories, San Diego, CA, USA) and cultured according to the manufacturer's instruction. All ICC-liver coculture was maintained in a 1:1 mixture of mouse HepatiCult™ Organoid Growth Medium (STEMCELL) and previously reported cholangiocyte organoid culture medium[17] supplemented with 1% GFR matrigel was used in all cocultures. AggreWell 400 (AW400) culture plates (STEMCELL Technologies, Vancouver, Canada) were used to generate ICC and

liver spheroids. Two-chamber culture insert and μ-slide 8-well Grid-500 culture slides from ibidi (Gräfelfing, Germany) were used in 2D coculture. See Supplementary Material for details.

ICC Orthotopic and Tail Vein Transplantation Models

For ICC orthotopic transplantation, PPTR-1 tumor cells were surgically injected into the liver of two-month-old male and female CD-1 nude mice at 1×10^5/mouse in 4 μl cold growth factor-reduced (GFR) matrigel (Corning). For tail vein injection (TVI)-based ICC lung metastasis model, PPTR-1 tumor cells were injected into two-month-old CD-1 nude mice at 1×10^6/mouse in 100 μl PBS via TVI.

IgG and Vcam1 antibody treatment

For in vivo assays, mice were treated three days after orthotopic or TVI transplantation with *InVivo*MAb anti-mouse CD106 (Vcam1) antibody ($Vcam1^{Ab}$) (Bioxcell, Lebanon, NH, USA) or rat IgG (R&D System, Minneapolis, MN, USA) at 0.25 mg/mice via TVI for 3 weeks, twice a week, five mice/group. For in vitro assays, cultured cells were treated with 10 μM $Vcam1^{Ab}$ or IgG for 4 days.

Reagents for Cell Labeling and Detection

All flow cytometric analyses were performed on a BD LSRFortessa™ cell analyzer (BD Biosciences) and Flow data were analyzed using FlowJo_V10. See Supplementary Material for details.

Vcam1 detection: APC anti-mouse CD106 (Vcam1) antibody (BioLegend, San Diego, CA, USA).

Cell proliferation: CellTracker™ Red CMTPX dye (Invitrogen, Carlsbad, CA, USA).

Cell apoptosis: NucView® 405 and NucView® 530 Caspase-3 Substrate (Biotium, Fremont, CA, USA).

Cytokine Array Assay

Conditioned media (CM) were collected from cell cultures after four days. The levels of secreted cytokines in the CM were measured using Mouse Cytokine Antibody Array 3 (RayBiotech, GA, USA) according to the manufacturer's instructions.

Immunohistochemistry analysis

Paraffin sections (4 μm) of liver spheroids and tissues were prepared by HistoWiz Inc. (Brooklyn, NY) and analyzed by direct fluorescence microscopy, H&E staining, and immunohistochemistry (IHC). Direct ZsG and TdT fluorescence images were taken from the sections prior to IHC. IHC antibodies included anti-Ki67 (Abcam, Cambridge, MA, USA, ab16667, 1:200); anti-CK19 (Abcam, ab133496, 1:250); anti-Vimentin (Abcam, ab92547, 1:500); anti-HNF4a (R&D System, Minneapolis, MN, USA, PP-K9218-00, 1:125); anti-Cyp3A (Abcam, ab3572, 1:500); anti-aSMA (Abcam, ab124964, 1:1000); Vcam1 (Abcam, ab134047, 1:1000) and anti-CD68 (Abcam, ab125212, 1:1000).

Microscopy, Image-based Quantification and Statistical Analysis

All cocultures were monitored daily by using an ECLIPSE Ts2R fluorescence microscope (Nikon, Minato City, Tokyo, Japan) and Lionheart FX Automated Microscope (Winooski, VT, USA). The ZsG^+ tumor cell area and TdT^+ HC area in cocultures were measured by Image J and plotted in GraphPad Prism 7. See Supplementary Material for details. Two-tailed student *t* test was performed in GraphPad Prism 7 to compare two independent pairs of groups. One-way ANOVA was performed when two or more groups were compared. *P* value ≤ 0.05 was considered statistically significant.

Transcriptomic analysis

We identified 103 significantly enriched gene sets from the GSEA results with these thresholds: significance p-value < 0.05 and |NES| > 1.5. We then graphically organized them into a network by the Cytoscape software (v3.8.2)[18] and the plugin Enrichment Map (v3.3.2, PMID: 21085593). See Supplementary Material for details.

RESULTS

HSCs are activated by ICC development in a temporal- and spatial-dependent manner

HSC activation within ICC tumors has been widely demonstrated,[8] but little is known about the activation status of HSCs in the tumor-surrounding liver. Therefore, we performed immunohistochemistry (IHC) of alpha-smooth muscle actin (αSMA), a well-recognized marker for activated HSCs, on three ICC patient tumors with >=5mm adjacent liver attached. We selected tumors resected without neoadjuvant treatment to exclude therapy-induced liver fibrotic reactions from our study. We found large numbers of A-HSCs in all three tumors as well as their surrounding peritumoral liver (**Figure 1A)**. Interestingly, we found A-HSCs were at a particularly high density at the tumor border in all three tumors compared to those in the tumor core or in the liver, suggesting tumor-liver interaction as an inducer of HSC activation.

Since HSC activation in the ICC patients could be triggered either by tumorigenesis or by other non-tumor-related preexisting conditions, we utilized an orthotopic allograft model of metastatic ICC we established in our laboratory to track ICC-induce spatial and temporal HSC activation. Using tumor cells cultured from a previously reported *Prom1*^{CreERT2}*; Pten*$^{flx/flx}$*; Tp53*$^{flx/flx}$*; Rosa-ZsGreen* (PPTR) liver cancer genetic model,[16, 19] we acquired two tumor cell lines, PPTR-1 and -2 which developed metastatic tumors with classic ICC histology (**Suppl Figure S1A-C**). The *Rosa-ZsGreen* (*ZsG*) reporter allele in the PPTR tumor cells enabled direct visualization of the gross tumor metastasis as well as disseminated tumor cells (DTCs) on tumor sections (**Suppl Figure S1D**). We collected the ICC allograft tumors and age-matched wildtype livers from different time points and performed αSMA IHC. As expected, normal mouse liver had very few A-HSCs (**Figure 1B, a**). In the early-stage ICC tumors developed after 2 weeks (2-wk) post transplantation, A-HSCs were found primarily at the tumor-liver border (**Figure 1B, b**). In tumors collected after one month (1-mon), we found a large number of A-HSCs mainly residing at the tumor periphery. A-HSCs were also seen in the tumor core, however, at a significantly lower number than those at the periphery. HSCs in the liver that were not in direct contact with the tumor mass remained largely quiescent although small intrahepatic metastases and activated HSCs on their border could be found at

this stage (**Figure 1B, c, d**). In the 3-mon tumors, extensive distribution of A-HSCs could be found in- and outside of the tumor including the liver near and far from the tumor mass (**Figure 1B, e-h**). Therefore, we found there was a spatial and temporal activation of HSCs induced by ICC development in our ICC mouse model.

Since previous studies have predominantly shown that A-HSCs promote liver tumor growth,[6, 7, 20] we examined tumor cell proliferation in our allograft tumors in association with the A-HSC content. Surprisingly, we found tumor cells in the A-HSC^{high} regions at the tumor periphery in the 1-mon allograft tumors had significantly fewer Ki67^{+} cells than those in the A-HSC^{low} regions in the tumor core. (**Figure 1C, a-j**, and **Figure 1D**). In the 3-mon tumors where a large number of itHSCs were present in the tumor core, we noticed a strong, positive association between A-HSC content and Ki67 positivity (**Figure 1C, k-t** and **Figure 1D**). However, at the tumor border where peritumoral (ptHSCs) accumulated, we found low tumor cell proliferation rate similar to the A-HSC^{low} regions in the tumor core (**Figure 1C, p-t**, and **Figure 1D**). These results suggest that intratumoral HSCs (itHSCs) promote tumor growth as previously reported. But ptHSCs are potentially growth-suppressive.

Tumor-liver spheroid coculture recapitulates HSC activation at the tumor-liver border

Because tumor-associated changes in vivo were part of a systemic response of the liver that could be shaped by non-hepatic lineages, we developed an in vitro tumor-liver spheroid coculture model to detemine if the initial HSC activation we observed at the tumor border was induced directly by ICC-liver interaction. Normal hepatocytes (HCs) and whole liver cells (WLCs) were isolated from *Rosa*$^{tdTomato/GFP}$ (*mTmG*) mice and cultured in AggreWell400 (AW400) plates for 7 days to generate spheroids (**Suppl Figure S2A**). All cells from mTmG mice expressed a strong *tdTomato* (TdT) red fluorescence protein (RFP). IHC characterization confirmed the presence of HNF4α^{+} HCs and small numbers of αSMA^{+} HSCs, CD68^{+} Kupffer cells, and CK19^{+} cholangiocyte in the WLC spheroids (**Figure 2A**). ICC tumor spheroids could be readily generated in the same way within 2 days (**Suppl Figure S2B**). To model

tumor-liver interaction, ICC spheroids were mixed with the HC or WLC spheroids at a ratio of 1:15, or by themselves, referred to as WLC-T, HC-T and T-only culture respectively (**Figure 2B**). All spheroids aggregated by 48 hr and ZsG^+ tumor area expanded steadily in all three cultures. However, we noticed that the ZsG^+ area expanded most slowly in the WLC-T culture while at a higher and similar rate in the T-only and HC-T cultures (**Figure 2C**). We collected the spherhoids after 7 days and performed IHC characterization. Compared to the HC-T spheroids, WLC-T spheroids showed a marked accumulation of αSMA^+ A-HSCs at the tumor-WLC spheroid border indicating an activation of HSCs upon direct WLC-ICC cell contact (**Figure 2D, a-d**). Additionally, similarly to our observations in the 1-mon allograft tumors, tumor cells close to the $A\text{-}HSC^{high}$ border in the WLC-T spheroids appeared to be less proliferative than those in the $A\text{-}HSC^{low}$ region (**Fig. 2D, e-h**), suggesting a potential growth suppressive role of ptHSCs which we assessed further below.

Peritumoral HSCs suppress, and intratumoral HSCs promote, ICC cell growth

We developed a "2.5-dimensional" (2.5D) coculture system to assess the effect of itHSCs and ptHSCs on ICC growth (**Figure 3A**). Primary HSCs were purchased and cultured in 2D condition to activate.[21] ICC cells were labeled with CellTracker™ Red CMTPX dye (CellTracker-RFP) to monitor their proliferation as CellTracker-RFP would be diluted into daughter cells upon cell division and lower RFP intensity would indicate faster cell proliferation. CellTracker-RFP-labeled ICC cells were then used to generate tumor (T)-spheroids, or mixed at 1:1 with primary HSCs to generate T+HSC-spheroids. The bottom layer of the 2.5D coculture was prepared by culturing freshly isolated HCs, a 1:1 mixture of HC+HSC, or HSCs in 2D condition in 96-well microplates. The bottom layer was allowed to attach for 24 hr and T- and T+HSC-spheroids were added on the top at 2-5 spheroids/well. We instantly noticed a slowed expansion of the ZsG^+ tumor area in the conditions with HSCs in the bottom layer (**Figure 3A, a-l**). When we seeded T-spheroids on top of the HC+HSC layer mixed at additional ratios, we noticed a significant and reversed association between the expansion rate of the ZsG^+ area and the HSC content in the bottom layer (**Suppl Figure S3A, B**). This trend was consistent although less obvious in the T+HSC-spheroid

2.5D cocultures (**Figure 3A, m-x**). All cells were collected after four days of coculture and examined for their CellTracker-RFP levels. In both T- and T+HSC-spheroid cultures, tumor cells placed on top of HSCs had the most RFP^+ cells (**Figure 3B)** as well as the highest RFP intensity (**Figure 3C)**, indicating their slowest proliferation compared to the other conditions. Tumor cells on top of HC+HSC had the second slowest proliferation rate while those on the top of HCs or no bottom layer grew at a similarly high rate (**Figure 3B, C**). Interestingly, when comparing T- and T+HSC-spheroids placed on the same bottom layer, tumor cells in the T+HSC-spheroids showed consistently higher proliferation rate indicated by their lower levels of CellTracker-RFP (**Figure 3B, C**). These results are consistent with our observations in the ICC allograft tumors that there is an intriguing, spatial-specific effect of HSCs on ICC growth, i.e. itHSCs promote tumor growth and ptHSCs suppress tumor cell proliferation.

Elongated ICC-ptHSC interaction elicits ICC cell dissemination

Since ptHSCs have been shown to be associated with poor prognosis in HCC patients, we wondered whether the growth-suppressive ptHSCs might eventually elicit aggressive behaviors from tumor cells. To test this, we continued monitoring the 2.5D cocultures up to 6 weeks (**Figure 4A** and **Suppl Figure S3A, D**). We noticed that T-spheroids placed on top of HSC-containing bottom layers grew very slowly but started showing evident invasion and dissemination from the spheroid surface by Day 14 (D14) (**Figure 4A, a-h**). Higher HSC content on the bottom was associated with more extensive invasion and dissemination (**Suppl Figure S3A, C**). Interestingly, T+HSC-spheroids, although bigger, were less invasive than the T-spheroids seeded in the same conditions (**Figure 4A, i-p**), suggesting that itHSCs promote tumor growth but not invasion or dissemination.

To better visualize ptHSC-induced tumor cell invasion, we developed a 2D tumor-liver coculture system using a two-chamber culture insert to spatially separate tumor and liver cells (the left and right chamber will be referred to as C1 and C2, respectively). (**Figure 4B**). A stable 2D HC cell line was established for this assay using primary HCs isolated from a *mTmG* mouse. Different combinations of HC, HSCs, and

ICC cells were seeded as shown in **Figure 4B** in culture slides engraved with a 500 μm-grid to track tumor cell movement. The insert was removed after 24hr to allow cells to grow and interact. Similar to our observations from the 2.5D cocultures, itHSCs promoted ICC cell growth in this two-chamber cocultures when tumor cells and HSCs were mixed in C1 and C2 was left empty (**Figure 4B, a-c vs. d-f**, and **Figure 4C**). However, this effect disappeared when HCs were placed in C2 which significantly slowed down tumor cell expansion after they encountered although tumor cells were able to progressively invade into the HCs and continue to grow (**Figure 4C, g-i vs. j-l** and **Figure 4C**). Interestingly, we noticed a further reduced tumor cell invasion into the HCs when HSCs were mixed with HCs in C2, however, a significant increase in tumor cell dissemination by D14 (**Figure 4B, m-o** and **Figure 4C**). Tumor cell invasion and dissemination was further increased when only HSCs were seeded in C2 (**Figure 4B, p-r**). Similar to these in vitro observations, the 3-mon metastatic tumors consistently had a high density of ptHSCs at the border where disseminating tumor clones appeared compared to the intact borders (**Figure 4D**), supporting the notion that ptHSCs at tumor border promote tumor cell invasion and dissemination.

Peritumoral HSC protect hepatocytes from DTC-induced cell death

Another intriguing observation in the two-chamber cocultures was a significant loss of HCs which occurred at a faster rate in T(C1):HC(C2) culture than T:HC+HSC (**Figure 4B, h&k vs. n**, and **Figure 5A**), which suggests a HC-killing effect of ICC cells and a hepatoprotective role of ptHSCs. We confirmed that the loss of HCs was at least partially via apoptosis (**Suppl Figure 4A**) and HCs cultured without ICC cells showed no cell death (**Supple Figure 4B**). We then confirmed that ICC cells were able to induce rapid HC death when they were put in 3D organoid coculture (**Figure 5B**). In the 1-mon ICC allograft tumors where ptHSCs were yet activated, we also spotted small peritumoral areas showing DTC-associated HC death (**Figure 5C, a, b**). In the 3-mon ICC allograft tumors where DTCs were wide-spreading in the liver, we found HC death was surprisingly limited. Interestingly, there was also an extensive activation of ptHSCs which spatially coincided with the DTCs (**Figure 5C, c, d**), suggesting

activated ptHSCs were potentially hepatoprotective. To test this hypothesis, we seeded HCs or HC+HSC (1:1) with a small number of ICC cells (approximately 20 tumor cells/chamber) to model DTC-liver interaction. Indeed, HC death was significantly reduced in HC+HSC:DTC culture compared to HC:DTC culture (**Figure 5D, E**), supporting a hepatoprotective role of activated ptHSCs.

Peritumoral HSCs induce Vcam1 upregulation in ICC cells which fine tunes tumor growth and metastasis

Next, we investigated the potential molecular mechanism involved in ICC-ptHSC interaction. Since cytokines are known key players in fibroblast-associated tumor invasion and metastasis,[22, 23] we performed a cytokine array assay using conditioned media (CM) collected from D4 T (top):HC(bottom), and T:ptHSC 2.5D cocultures (**Suppl Figure 5A**). We noticed a mild but significant increase in Vascular Cell Adhesion Molecule 1 (Vcam1) in T:HSC CM compared to the others (**Figure 6A**). Vcam1 has been previously implicated in increasing solid tumor metastasis,[24, 25] and we have reported that Vcam1 was associated with tumor metastasis in our allograft model.[16] Via flow cytometry, we confirmed the increase in $Vcam1^+$ tumor cells in D4 T:ptHSC coculture (**Suppl Figure 5B**). To determine the potential contribution of Vcam1 to tumor cell dissemination occurring late in this model, we also examined Vcam1 levels in D42 cocultures when tumor cells in the T:HSC coculture had displayed extensive dissemination (see **Suppl Figure S3D**). Surprisingly, Vcam1 levels were significantly lower in the tumor cells from all three D42 cocultures compared to D4 (**Figure 6B**), suggesting Vcam1 expression was not driving the dissemination phenotype in the T:HSC coculture. In the1-mon ICC allograft tumors, we found a consistent upregulation of Vcam1 at the tumor periphery, the same areas where A-HSCs were enriched (**Figure 6C, a-e**). In the 3-mon allograft tumors, higher Vcam1 expression was also found in the tumor cells at the borders where ptHSCs accumulated than those within the tumor core (**Figure 6C, f-i**). However, DTCs in the peritumoral liver were all Vcam1-negative (**Figure 5C, j-**k). In the ICC patient tumors, Vcam1-expressing tumor cells were similarly found to be generally higher in the tumor cells at

the borders where pHSCs were present than those within the tumor core (**Suppl Figure S6**). We could not evaluate Vcam1 expression in the DTCs in patient tumors due to the lack of approaches to detect DTCs.

Based on the temporal and spatial dynamics of Vcam1 expression in vitro and in vivo, we suspected that Vcam1 contributes to ICC aggressiveness indirectly by protecting tumor cells from the suppressive environmental elements including ptHSCs. But its function as an adhesion molecular would have a negative impact on tumor cell dissemination. We were not able to test this hypothesis by genetically manipulating Vcam1 in our ICC cells since these cells had shown strong resistance to transduction. A small subpopulation of ICC cells that we were able to transduce produced tumors with a different histopathology (data not shown). Therefore, we chose to use a reported Vcam1 neutralizing antibody to block Vcam1 activity.[26] Consistently with our hypothesis, ICC cells treated with the Vcam1 neutralizing antibody ($Vcam1^{Ab}$) showed reduced migration in vitro (**Suppl Figure S5C**) but no changes in their proliferation or apoptosis (**Suppl Figure S5D, E**). In the orthotopic model treated with $Vcam1^{Ab}$ or IgG for three weeks, we found tumors in the $Vcam1^{Ab}$ group were smaller than those in the IgG-treated, suggesting a reduced growth potential of the tumor when Vcam1 was blocked. However, $Vcam1^{Ab}$-treated tumors appeared to be more disseminating with more small disseminating tumor clones on the border (**Figure 6D)** and more DTCs in the lung (**Suppl Figure 7A**). We were aware that metastasis outcome in orthotopic allograft models did vary between mice. Therefore, we further validated the dissemination-suppressing role of Vcam1 in the allograft model via a tail vein injection (TVI) lung metastasis model. ICC cells were injected into mice via TVI and biweekly $Vcam1^{Ab}$ or IgG treatment was started on Day 3 after tumor seeding had completed. Lung metastasis outcome was examined after three weeks. Once again, we found mice treated with $Vcam1^{Ab}$ consistently developed more lung metastases than those treated with IgG (**Figure 6E** and **Suppl Figure 7B**). Interestingly, the size of the lung metastases in the IgG-treated mice was larger than those in the $Vcam1^{Ab}$-treated mice (**Figure 6F**) while the latter developed a significantly higher number of small metastases (**Figure 6G**). IHC showed that in both groups, larger metastases had lower Vcam1 expression than the smaller ones, and the DTCs around

the metastases were consistently Vcam1-negative (**Figure 6H, a-f**). Vcam1 levels were lower in $Vcam1^{Ab}$-treated tumors than IgG-treated tumors in general but not completely depleted, suggesting a partial Vcam1 blocking potentially due to the high tumor burden in this model (**Figure 6H, e, f**). Additionally, $Vcam1^{high}$ tumor areas had consistently more interacting αSMA^{+} fibroblasts than the $Vcam1^{low}$ areas in both groups (**Figure 6F, e-h**), suggesting a similar association between tumor-fibroblast interaction and Vcam1 expression in the lung metastases as seen in the liver allograft tumors. Overall, our observations from both liver orthotopic transplantation and TVI lung metastasis models suggest that Vcam1 plays an important role in supporting tumor growth in both liver and lung but Vcam1 needs to be turned off for tumor cells to successfully disseminate from the established tumor mass.

ICC development induces broad metabolic, oncogenic, and immune changes in peritumoral liver

Lastly, we performed total RNA-sequencing using peritumoral livers from late-stage metastatic ICC allograft tumors and non-tumor bearing, age-matched mouse livers to investigate the overall peritumoral changes induced by ICC development. We confirmed the upregulation of additional HSC markers in the peritumoral liver of the allograft tumors including *Des* (encodes desmin),[27] *Pdgfr1*[28] and *Pgfgr2*[29] (**Figure 7A**). When comparing to a reported 37-gene peritumoral A-HSC signature associated with HCC patient survival,[14] we found 6 of them being significantly upregulated in our allograft model and additional 13 genes whose family members were significantly upregulated (**Suppl Table S1**). Intriguingly, GSEA analysis found a large number of differential expressed gene sets in the peritumoral liver of the allograft tumors in three major fields: liver metabolism, cancer development and immune activation **(Figure 7B** and **Suppl Table S2**). Downregulation of gene sets regulating liver metabolism were among the most significant changes induced by ICC development, indicating a disrupted function of ICC-bearing liver, consistent with the hepatoxicity of ICC tumor cells we observed in vitro (see **Figure 4**). H&E on both mouse and patient ICC tumors confirmed the presence of damaged HCs, proliferative HCs and infiltration of T cells and macrophages in the peritumoral liver of both mouse and patient tumors (**Figure 7C**). These results demonstrate a broad ICC-induced peritumoral changes beyond HSC activation.

DISCUSSION

Using an orthotopic model of metastatic ICC and a number of novel multi-lineage cellular models we established in the laboratory, we showed that there were intriguing temporal and spatial dynamics of HSC activation during ICC development. At the early stage of ICC tumorigenesis, HSCs were rapidly activated at the tumor-liver border. When tumor gets larger, there is an increase in the activated itHSCs within the tumor as well as an expansion of ptHSCs extending from the tumor border into the liver. We found itHSCs and ptHSCs play distinct roles on tumor growth. Activated itHSCs are growth-promoting as previously reported,[6, 7] while ptHSCs exhibit a surprising growth-suppressive effect on ICC cell proliferation. However, we found prolonged ptHSC-ICC interaction at the tumor border induce tumor cell invasion and dissemination, which is in line with the previous observations in liver cancer patients that activated ptHSCs are associated with tumor metastasis and relapse.[14, 15] Our study also finds that further ptHSC activation in the peritumoral liver of late-stage metastatic ICC spatially coincide with DTC spreading and the ptHSCs exert a strong protective effect on hepatocytes from DTC-induced cell death.

Based on our study, we propose that the initial HSC activation is likely a defensive response of the liver to tumorigenesis, intended to restrain local tumor growth and, in turn, preserve liver function. Indeed, recent studies have started to argue that cirrhosis, a late-stage liver fibrosis condition that heavily involves HSC activation, may be a liver-protective response rather than a risk factor for live cancer.[30] Depletion of HSCs at the early stage would potentially dampen liver's ability to effectively suppress tumor growth and lead to accelerated tumor development. However, we find protumorigenic itHSCs are highly abundant in late-stage tumors and we propose their depletion at this stage would slow tumor progression. We suspect that the different timing of fibroblasts depletion may account for, at least partially, to the different tumor outcomes in the previously reported CAF-depletion studies.[7, 12, 31-33] A genetic approach capable of a temporal- and spatial-specific depletion of HSCs, when it becomes available, would be the most definitive in defining their role in ICC development. A single-cell transcriptomic analysis using our coculture

systems and mouse models in the future will also be necessary to pinpoint the molecular mechanisms behind the differential roles of itHSCs and ptHSCs play in ICC-HSC interaction.

Our study find, however, that the growth suppression by ptHSC has a devastating adverse consequence which is the eventual elicitation of more aggressive behaviors from tumor cells leading to tumor cell dissemination, an observation in line with the role of cell competition in selecting aggressive cancer behaviors.[34] ICC and many aggressive solid tumors are known to be highly heterogeneous and plastic, and tumor cells can readily change their behaviors depending on the environmental cues they receive. The suppression of ptHSC on tumor border likely leads to a selection process for aggressive ICC cells while attempting to contain tumor growth.[35] Tumor dissemination elicits further activation of HSCs in the liver to protect hepatocytes accompanied by a broad range of immune and oncogenic activation in the host liver in response to tumorigenesis. Although we lack tools to efficiently detect DTCs in ICC patient tumors as we do for our mouse models, the high rates of intrahepatic and distant tumor relapse in ICC patients, even after curative resection, suggests that tumor dissemination is common in these patients early in the clinical course, which could potentially be elicited by the large ptHSC population in ICC.

Since itHSCs have been widely studied for liver cancer, we focused on ptHSC in this study for the molecular investigation. We show that Vcam1 is upregulated in the tumor cells at the early phase of ICC-ptHSC interaction but drops when tumor cells start to disseminate. Although Vcam1 has been previously shown as a metastasis promoter,[24, 25] our tracking of Vcam1 expression in early-stage and late-stage metastatic ICC allograft tumors suggests that its function is beyond pro- or anti-metastatic. Vcam1 facilitates the growth of the tumor mass in both liver and lung. But it negatively impacts tumor cell dissemination as Vcam1 blocking consistently increases the formation of DTCs and small disseminating clones in both liver and lung. We need to acknowledge that the ICC cells we used in this study are highly metastatic and it is possible that the dependency on Vcam1 may be different for tumor cells with different metastatic potential. It also needs to be noted that we used a systemic blocking approach to study Vcam1 function which does not allow us to differentiate the contribution of other Vcam1-expressing cells to the

metastasis outcome we observed.[24, 25] However, our study does raise doubt to the previous proposals on targeting VCAM1 to treat metastatic disease,[36] as our results suggest highly aggressive tumors may benefit from Vcam1 blocking to disseminate more efficiently. A more detailed understanding of the dynamic involvement of Vcam1 in the complex metastasis cascade is needed before we assess its therapeutic values.

Overall, our study shows tumor-HSC interaction is beyond simple pro- or anti-tumorigenic. We theorize that the metastatic phenotype is an ongoing competitive process between the attempt of ptHSCs to block local tumor growth and that of tumor cells to break through the suppression. Future studies are in line to identify specific mechanisms underlying this complex tumor-host crosstalk with a goal to simultaneously address local tumor growth and early steps in metastatic progression.

FIGURE LEGENDS

Figure 1. Temporal and spatial activation of pHSCs in mouse and patient ICC tumors.

(A, B) IHC of αSMA in the ICC patient tumors **(A)** and mouse allograft tumors **(B)**.

(C) ZsG (tumor cells, T^{ZsG})/Dapi fluorescence microscopy, aSMA and Ki67 IHC in the 1- and 3-mon ICC allograft tumors.

(D) Quantification of $Ki67^+$ cells in the indicated areas of the 1- and 3-mon ICC allograft tumors. No HSC-high regions present in the 1-mon tumors. Student *t*-test, *P* value *** <0.001, ****<0.0001.

Figure 2. HSC activation in the tumor-liver spheroid coculture.

(A) Generation of HC and WLC spheroids in AW400 plates and their histological characterization. Antibodies used are indicated and all histology images share the same 100 μm scale bar.

(B) Merged bright-field/ZsG (tumor cells)/TdT (normal liver cells) images of the indicated spheroid cocultures showing the expansion of tumor cell area.

(C) Quantification of the ZsG^+ tumor area in the indicated spheroid cocultures on Day 0, 3, and 7. Student *t*-test, *P* value ** <0.01; ns, not significant.

(D) ZsG/TdT fluorescence microscopy, αSMA and Ki67 IHC in HC-T and WLC-T spheroids collected 7 days after coculturing.

Figure 3. Peritumoral HSCs suppress, and intratumoral HSCs promote, ICC cell proliferation.

(A) Time course images of the ZsG^+ T- and T+HSC-spheroids in the 2.5D coculture with the indicated bottom layers. All images share the same 200 μm scale bar.

(B) Flow cytometry-based detection of the CellTracker-RFP dye of T- and T+HSC-spheroids placed on the indicated bottom layer. Note that RFP-negative are plotted to indicate tumor cells proliferation index. *P* values of the Student *t*-test between the indicated groups are shown in the table below.

(C) RFP intensity histogram of ICC tumor cells in the indicated groups. Note that FRP intensity is reversely correlated with cell proliferation rate.

Figure 4. Peritumoral HSCs at tumor border induce tumor cell dissemination.

(A) Low- and high-magnification ZsG fluorescence images of the T- and T+HSC-spheroids placed on the indicated bottom layer at Day 14. Images on the same row share the same scale bar.

(B) Day 0 and 14 ZsG/RFP fluorescence images of the indicated two-chamber cocultures. HSCs are labeled with CellTracker-RFP in the conditions with no HC^{TdT} (**d-f** and **p-r**). Note clonal tumor dissemination only occurs when HSCs are present in the C2 chamber (**m-f**).

(C) Measurement of the expansion distance of the tumor cell border in the indicated conditions. Student *t*-test, ns, non-significant, *P* value ** <0.01, ****<0.0001.

(D) ZsG(tumor cells)/Dapi fluorescence microscopy and αSMA IHC images showing the intact and disseminating tumor border in the 3-mon allograft tumor. Arrows in (**d**): disseminated tumor clones. All images share the same 100 μm scale bar.

Figure 5. Activated ptHSCs in the liver are hepatoprotective.

(A) Day 7, 10, and 14 TdT fluorescence images from the two-chamber coculture indicating a slower loss of HCs in the T:HC+HSC coculture than T:HC coculture.

(B) ZsG/TdT images of the T-HC organoid coculture showing ICC-induced HC death. Arrows in (**j-l**): dying HCs in contact with ICC tumor cells.

(C) ZsG/Dapi and αSMA IHC images showing the disrupted liver parenchyma (outlined) in the presence of DTCs in the 1-mon allograft tumor (**a, b**) and colocalization of the activated ptHSCs and DTCs in the 3-mon tumor (**c, d**). Asterisk: liver region with no DTCs and activated ptHSCs.

(D) ZsG/TdT images of the indicated cocultures showing a slower loss of HCs in the presence of HSCs. Dotted outline: HC seeding area.

(E) Quantification of the outlined HC^{TdT} area in **(D)**. Student *t*-test, *P* value **** <0.0001.

Figure 6. ICC-pHSC interaction induces Vcam1 upregulation in tumor cells.

(A) Quantification of the Vcam1 levels from the cytokine array using CM from the indicated 2.5 cocultures and control conditions. Student *t*-test, *P* value * <0.05.

(B) Histogram of Vcam1 level in the tumor cells from the indicated cocultures at Day 4 and 42 showing a decrease in Vcam1 levels in Day 42 cultures.

(C) Vcam1 and αSMA IHC in the indicated allograft tumors. Vcam1 and αSMA IHC images were taken from the same areas on the serial sections. Arrows in **(a)**: $Vcam1^{high}$ cells at the tumor periphery of the 1-mon allograft tumor. **(k)**: ZsG/Dapi image of the DTCs. All the scale bars are 100 μm.

(D) Gross liver ZsG and ZsG(tumor cells)/Dapi fluorescence images of the tumors from orthotopic allograft models treated with IgG or $Vcam1^{Ab}$ for three weeks. Arrows in **(c)**: ZsG^{+} micrometastases in the liver; arrows in **(d)**: small disseminating clones on the tumor border.

(E) Gross ZsG and ZsG(tumor cells)/Dapi images of the lung metastases collected from the ICC-TVI model treated with IgG or $Vcam1^{Ab}$ for three weeks.

(F) Quantification of the area of individual lung metastases areas from mice in **(E)** showing larger lung metastases in the IgG-treated mice**.** Student *t*-test, *P* value ****<0.0001.

(G) Histogram of the size distribution of the lung metastases from mice in **(E)** showing the larger number of small lung metastases in the $Vcam1^{Ab}$-treated mice.

(H) H&E, ZsG(tumor cells)/Dapi fluorescence, and Vcam1 and αSMA IHC on the lung metastases from mice in **(E)** showing decreased Vcam1 level in DTCs and colocalization of $Vcam1^{+}$ and $αSMA^{+}$ regions.

Figure 7. Tumor development induced a broad range of peritumoral changes in the ICC allograft model.

(A) Upregulation of the indicated HSC markers in the ICC-liver detected by RNAseq.

(B) A functional map of GSEA comparison between normal and ICC-bearing mouse livers. The red nodes represent the gene sets upregulated in the tumor-bearing livers than the normal livers, and the blue nodes are down-regulated gene sets. Node size is proportional to the absolute value of normalized enrichment

score and the edge thickness represents the similarity coefficient between the gene sets. The solid blue ovals represent the subgroups of functionally related gene sets.

(C) Histological validation of the peritumoral changes demonstrated in **(B)** in ICC patient and mouse allograft tumors. Stains are as indicated and all the scale bars are 100 μm.

REFERENCES

1. Banales JM, Marin JJG, Lamarca A, et al. Cholangiocarcinoma 2020: the next horizon in mechanisms and management. Nat Rev Gastroenterol Hepatol 2020;17:557-588.
2. Rizvi S, Khan SA, Hallemeier CL, et al. Cholangiocarcinoma — evolving concepts and therapeutic strategies. Nature Reviews Clinical Oncology 2018;15:95-111.
3. Benson AB, D'Angelica MI, Abbott DE, et al. Hepatobiliary Cancers, Version 2.2021, NCCN Clinical Practice Guidelines in Oncology. J Natl Compr Canc Netw 2021;19:541-565.
4. Sirica AE, Gores GJ, Groopman JD, et al. Intrahepatic Cholangiocarcinoma: Continuing Challenges and Translational Advances. Hepatology 2019;69:1803-1815.
5. Yin C, Evason KJ, Asahina K, et al. Hepatic stellate cells in liver development, regeneration, and cancer. J Clin Invest 2013;123:1902-10.
6. Okabe H, Beppu T, Hayashi H, et al. Hepatic stellate cells accelerate the malignant behavior of cholangiocarcinoma cells. Ann Surg Oncol 2011;18:1175-84.
7. Affo S, Nair A, Brundu F, et al. Promotion of cholangiocarcinoma growth by diverse cancer-associated fibroblast subpopulations. Cancer Cell 2021.
8. Vaquero J, Aoudjehane L, Fouassier L. Cancer-associated fibroblasts in cholangiocarcinoma. Curr Opin Gastroenterol 2020;36:63-69.
9. Affo S, Nair A, Brundu F, et al. Promotion of cholangiocarcinoma growth by diverse cancer-associated fibroblast subpopulations. Cancer Cell 2021;39:866-882 e11.
10. Guedj N, Blaise L, Cauchy F, et al. Prognostic value of desmoplastic stroma in intrahepatic cholangiocarcinoma. Mod Pathol 2021;34:408-416.
11. Robinson MW, Harmon C, O'Farrelly C. Liver immunology and its role in inflammation and homeostasis. Cell Mol Immunol 2016;13:267-76.
12. Madsen CD. Pancreatic cancer is suppressed by fibroblast-derived collagen I. Cancer Cell 2021;39:451-453.
13. Bataller R, Brenner DA. Liver fibrosis. J Clin Invest 2005;115:209-18.

14. Ji J, Eggert T, Budhu A, et al. Hepatic stellate cell and monocyte interaction contributes to poor prognosis in hepatocellular carcinoma. Hepatology 2015;62:481-95.

15. Jiang J, Ye F, Yang X, et al. Peri-tumor associated fibroblasts promote intrahepatic metastasis of hepatocellular carcinoma by recruiting cancer stem cells. Cancer Lett 2017;404:19-28.

16. Li L, Qian M, Chen IH, et al. Acquisition of Cholangiocarcinoma Traits during Advanced Hepatocellular Carcinoma Development in Mice. Am J Pathol 2018;188:656-671.

17. Hu H, Gehart H, Artegiani B, et al. Long-Term Expansion of Functional Mouse and Human Hepatocytes as 3D Organoids. Cell 2018;175:1591-1606 e19.

18. Cline MS, Smoot M, Cerami E, et al. Integration of biological networks and gene expression data using Cytoscape. Nat Protoc 2007;2:2366-82.

19. Zhu L, Finkelstein D, Gao C, et al. Multi-organ Mapping of Cancer Risk. Cell 2016;166:1132-1146 e7.

20. Song Y, Kim SH, Kim KM, et al. Activated hepatic stellate cells play pivotal roles in hepatocellular carcinoma cell chemoresistance and migration in multicellular tumor spheroids. Sci Rep 2016;6:36750.

21. Mederacke I, Dapito DH, Affo S, et al. High-yield and high-purity isolation of hepatic stellate cells from normal and fibrotic mouse livers. Nat Protoc 2015;10:305-15.

22. Kalluri R. The biology and function of fibroblasts in cancer. Nat Rev Cancer 2016;16:582-98.

23. Calon A, Tauriello DV, Batlle E. TGF-beta in CAF-mediated tumor growth and metastasis. Semin Cancer Biol 2014;25:15-22.

24. Wieland E, Rodriguez-Vita J, Liebler SS, et al. Endothelial Notch1 Activity Facilitates Metastasis. Cancer Cell 2017;31:355-367.

25. Chen Q, Zhang XH, Massague J. Macrophage binding to receptor VCAM-1 transmits survival signals in breast cancer cells that invade the lungs. Cancer Cell 2011;20:538-49.

26. Chow A, Huggins M, Ahmed J, et al. CD169(+) macrophages provide a niche promoting erythropoiesis under homeostasis and stress. Nat Med 2013;19:429-36.

27. Nitou M, Ishikawa K, Shiojiri N. Immunohistochemical analysis of development of desmin-positive hepatic stellate cells in mouse liver. J Anat 2000;197 Pt 4:635-46.

28. Kikuchi A, Singh S, Poddar M, et al. Hepatic Stellate Cell-Specific Platelet-Derived Growth Factor Receptor-alpha Loss Reduces Fibrosis and Promotes Repair after Hepatocellular Injury. Am J Pathol 2020;190:2080-2094.

29. Kocabayoglu P, Lade A, Lee YA, et al. beta-PDGF receptor expressed by hepatic stellate cells regulates fibrosis in murine liver injury, but not carcinogenesis. J Hepatol 2015;63:141-7.

30. Garrido A, Djouder N. Cirrhosis: A Questioned Risk Factor for Hepatocellular Carcinoma. Trends Cancer 2021;7:29-36.

31. Chen Y, Kim J, Yang S, et al. Type I collagen deletion in alphaSMA(+) myofibroblasts augments immune suppression and accelerates progression of pancreatic cancer. Cancer Cell 2021;39:548-565 e6.

32. Rhim AD, Oberstein PE, Thomas DH, et al. Stromal elements act to restrain, rather than support, pancreatic ductal adenocarcinoma. Cancer Cell 2014;25:735-47.

33. Ozdemir BC, Pentcheva-Hoang T, Carstens JL, et al. Depletion of carcinoma-associated fibroblasts and fibrosis induces immunosuppression and accelerates pancreas cancer with reduced survival. Cancer Cell 2014;25:719-34.

34. Parker T, Madan E, Gupta K, et al. Cell Competition Spurs Selection of Aggressive Cancer Cells. Trends Cancer 2020;6:732-736.

35. Meacham CE, Morrison SJ. Tumour heterogeneity and cancer cell plasticity. Nature 2013;501:328-37.

36. Chen Q, Massague J. Molecular pathways: VCAM-1 as a potential therapeutic target in metastasis. Clin Cancer Res 2012;18:5520-5.

Figure 1

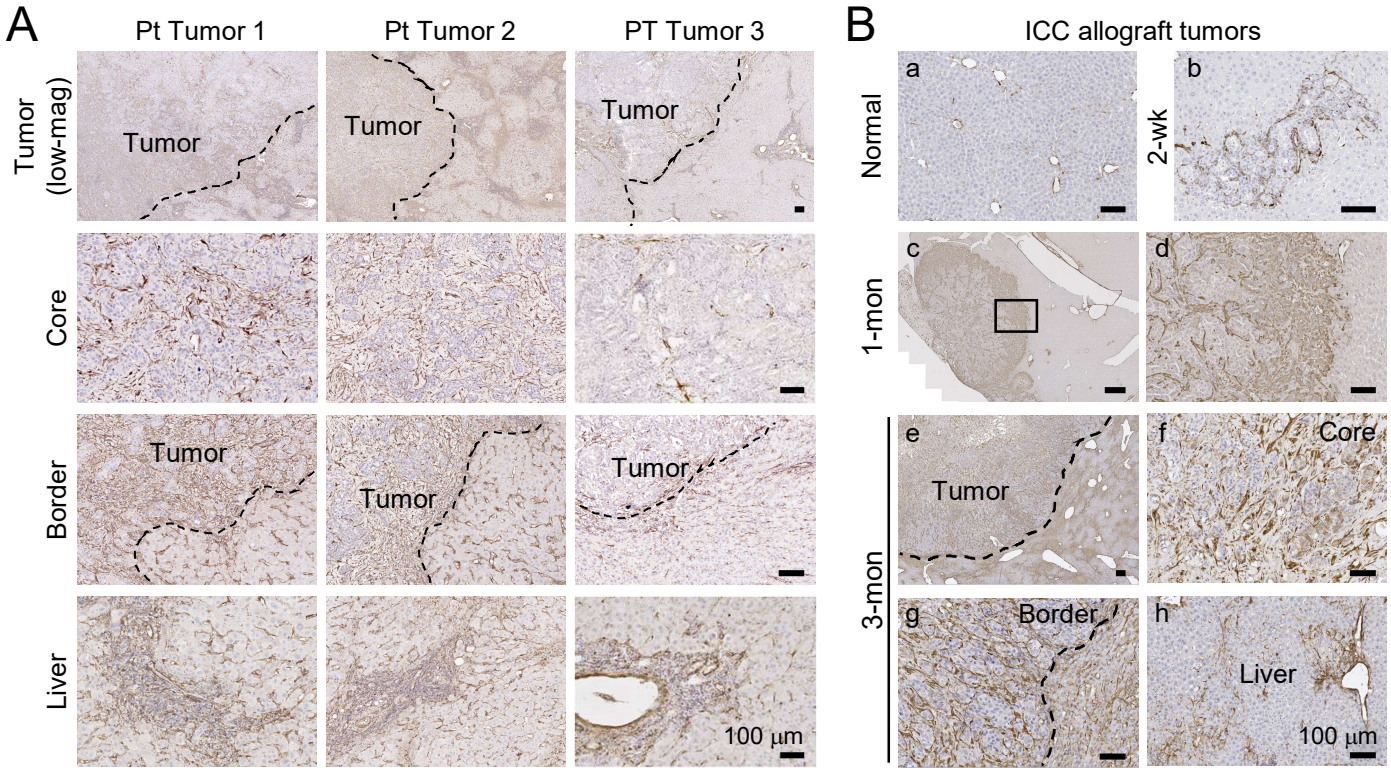

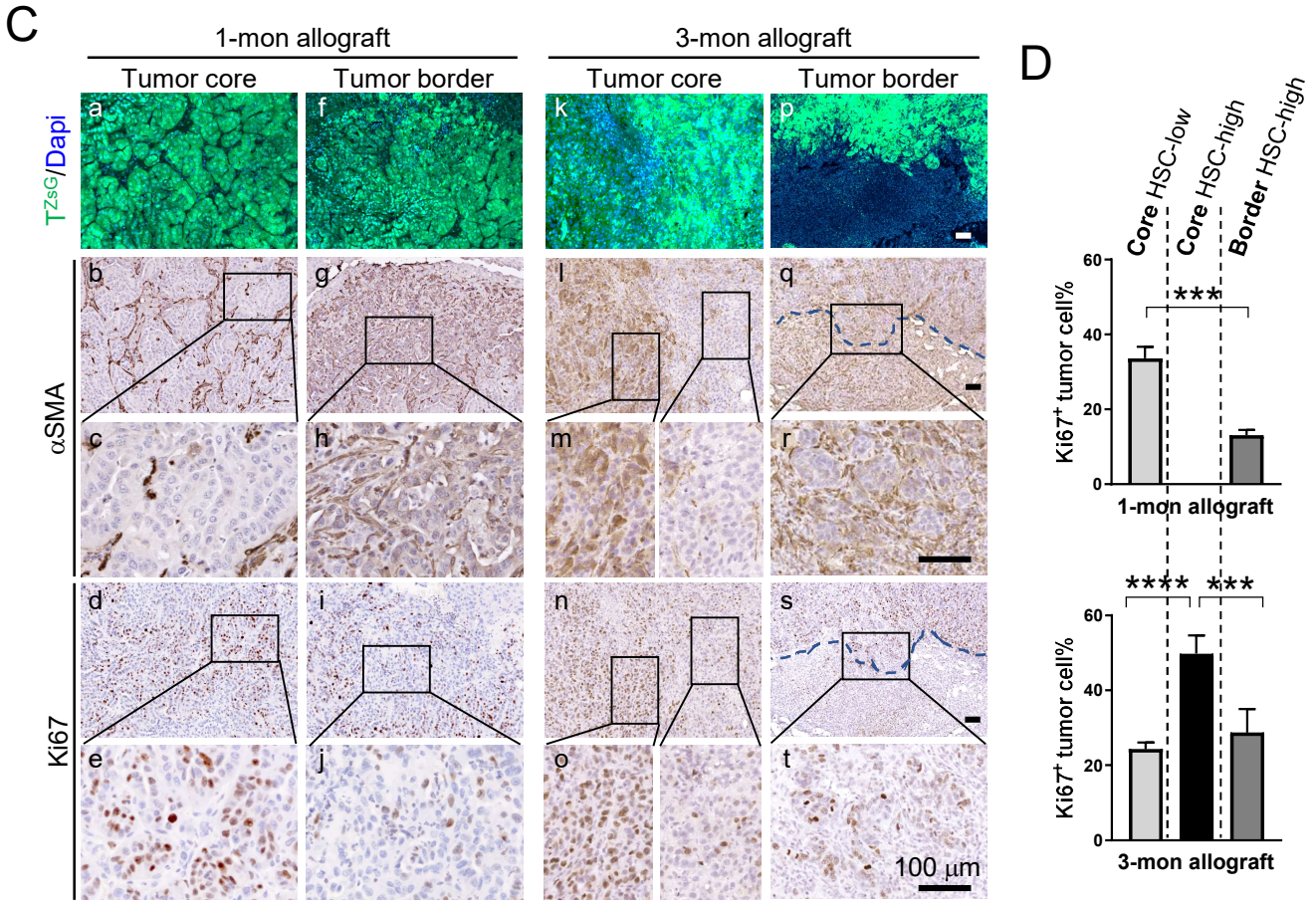

Figure 2

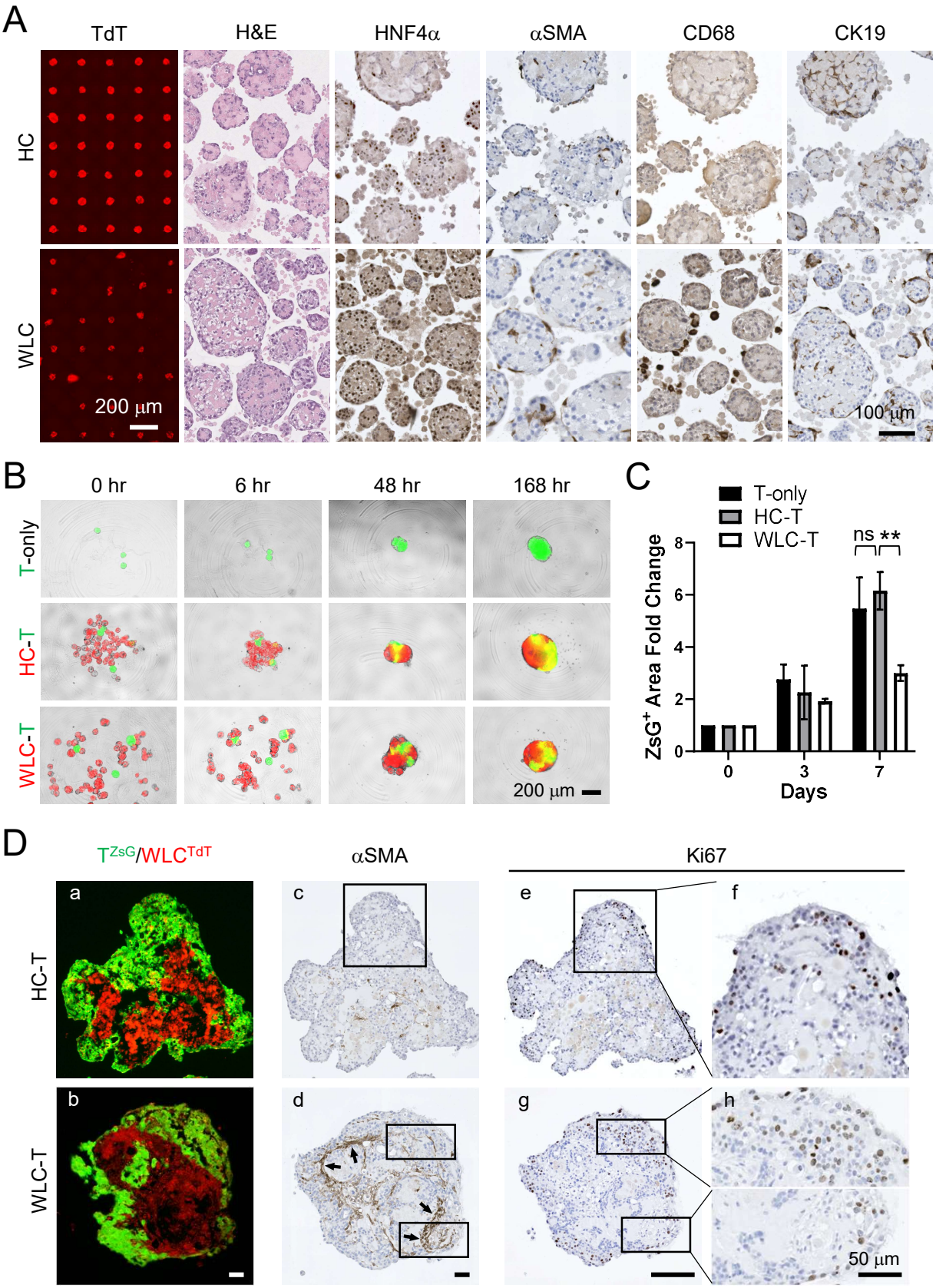

Figure 3

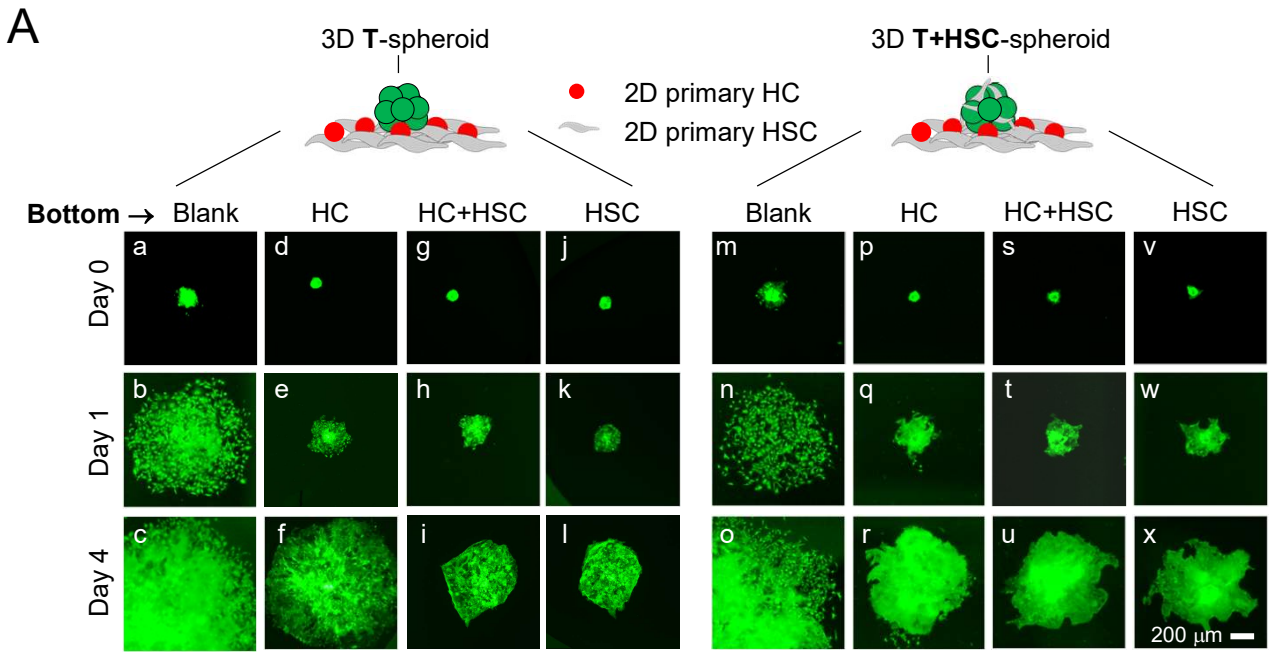

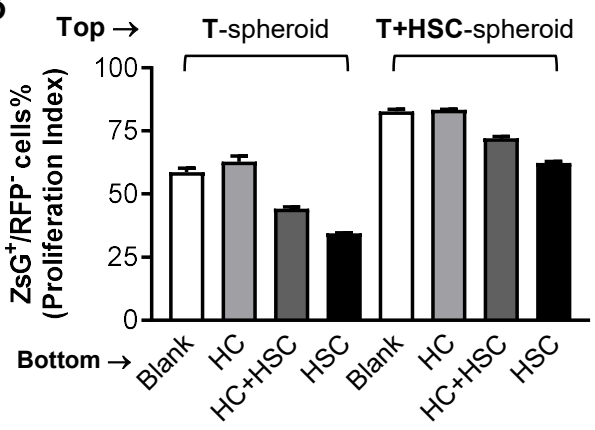

P value			T+HSC spheroid			
			5 Blank	6 HC	7 HC+HSC	8 HSC
				ns (6 vs 5)	<0.0001 (7 vs 6)	<0.0001 (8 vs 7)
T spheroid	1 Blank		<0.0001 (5 vs 1)			
	2 HC	ns (2 vs 1)		<0.0001 (6 vs 2)		
	3 HC+HS	<0.0001 (3 vs 2)			<0.0001 (7 vs 3)	
	4 HSC	<0.0001 (4 vs 3)				<0.0001 (8 vs 4)

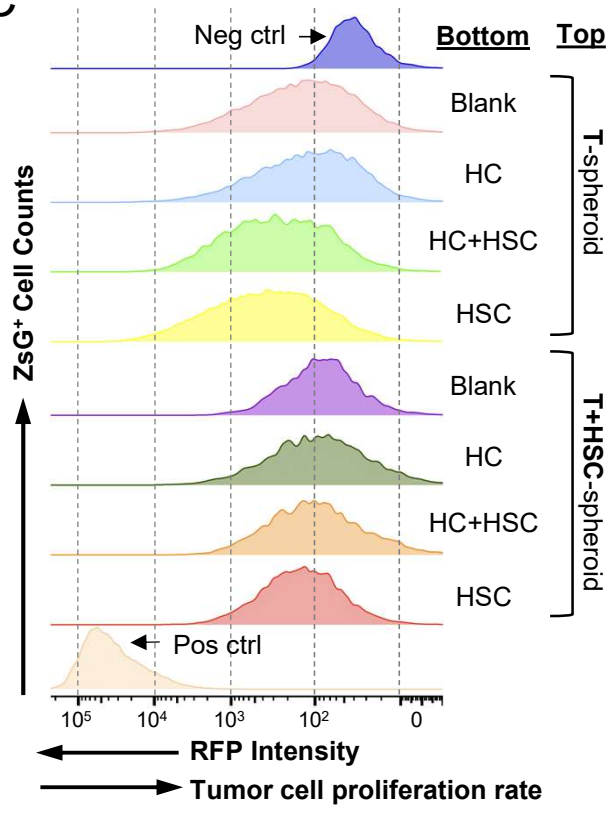

Figure 4

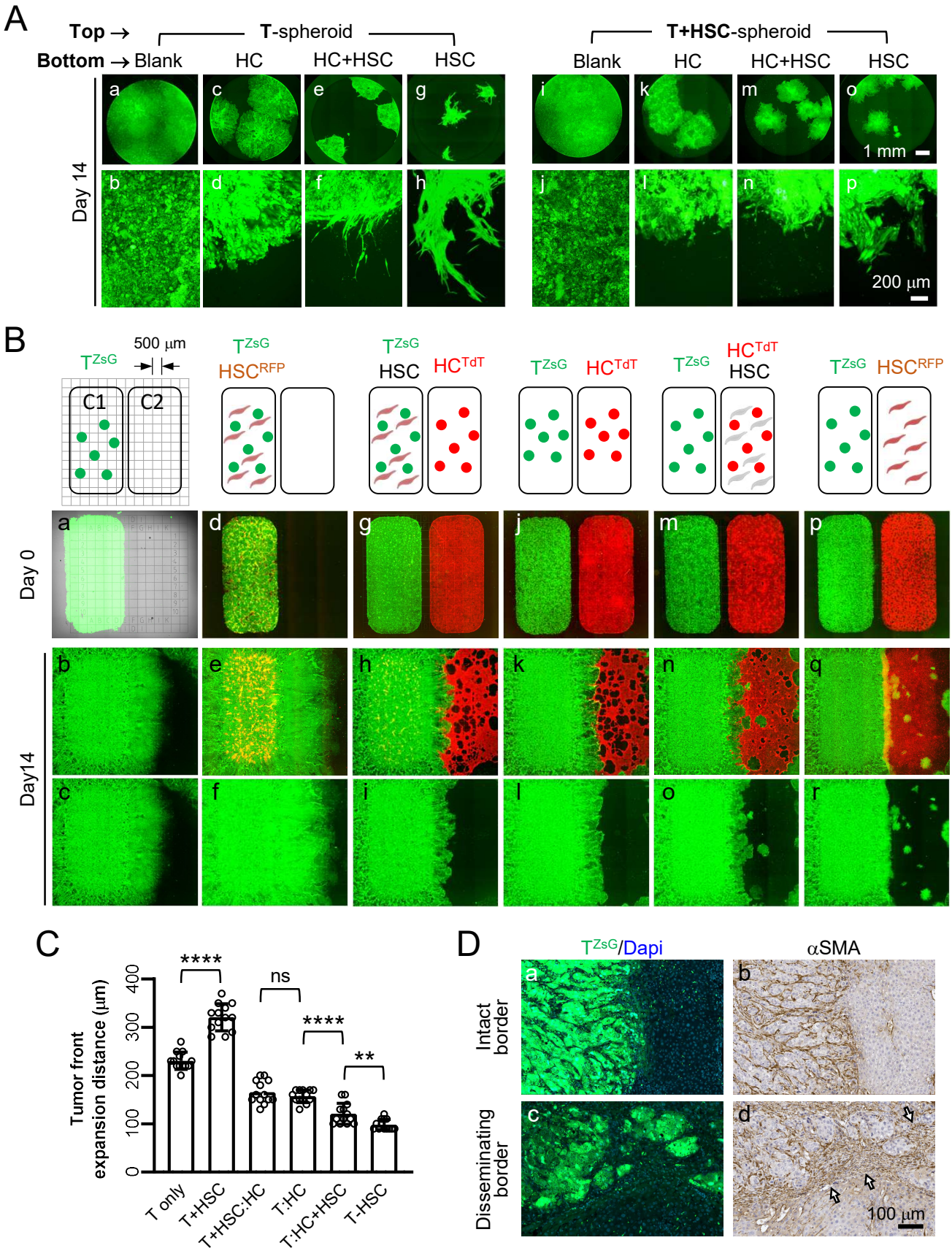

Figure 5

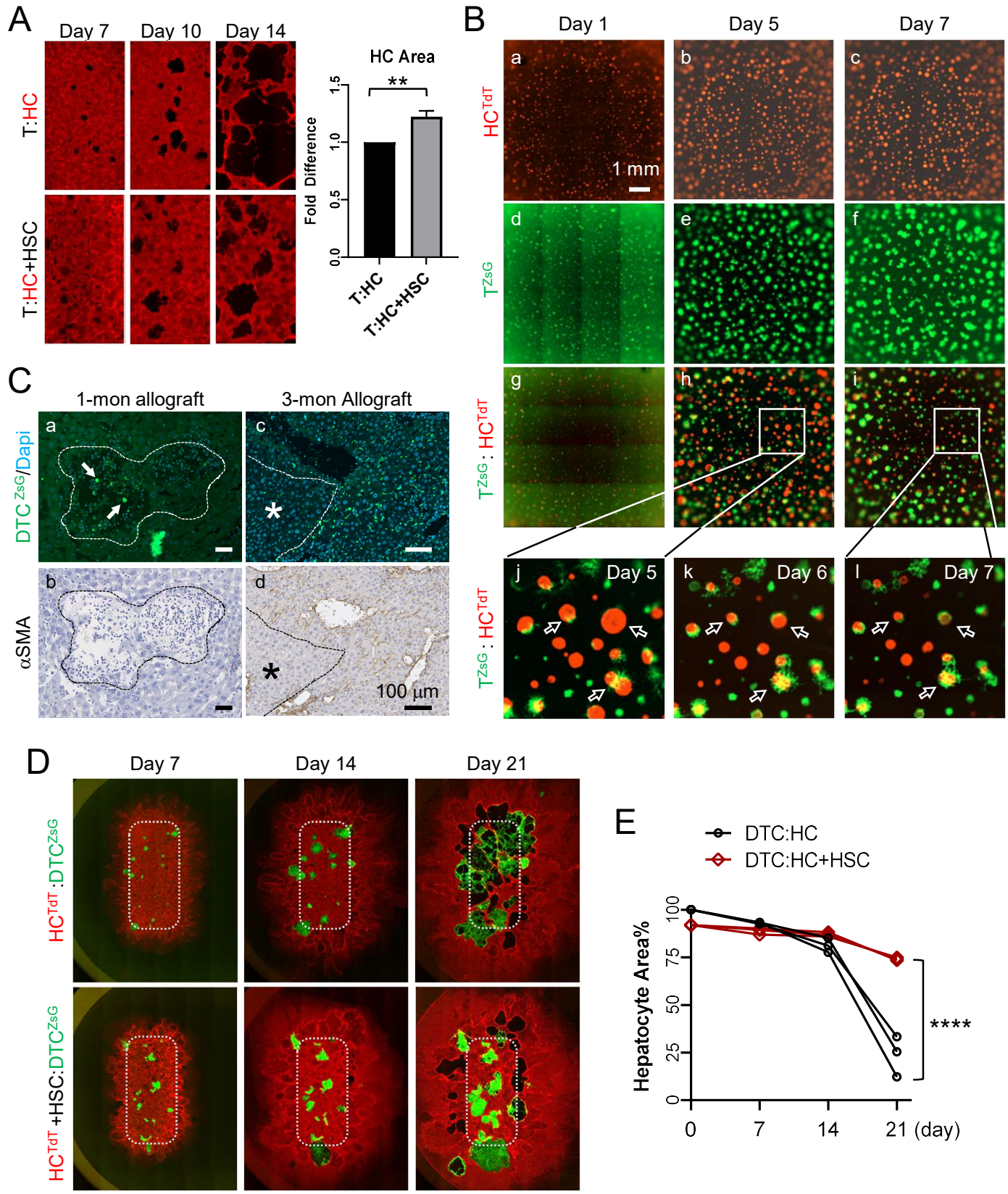

Figure 6

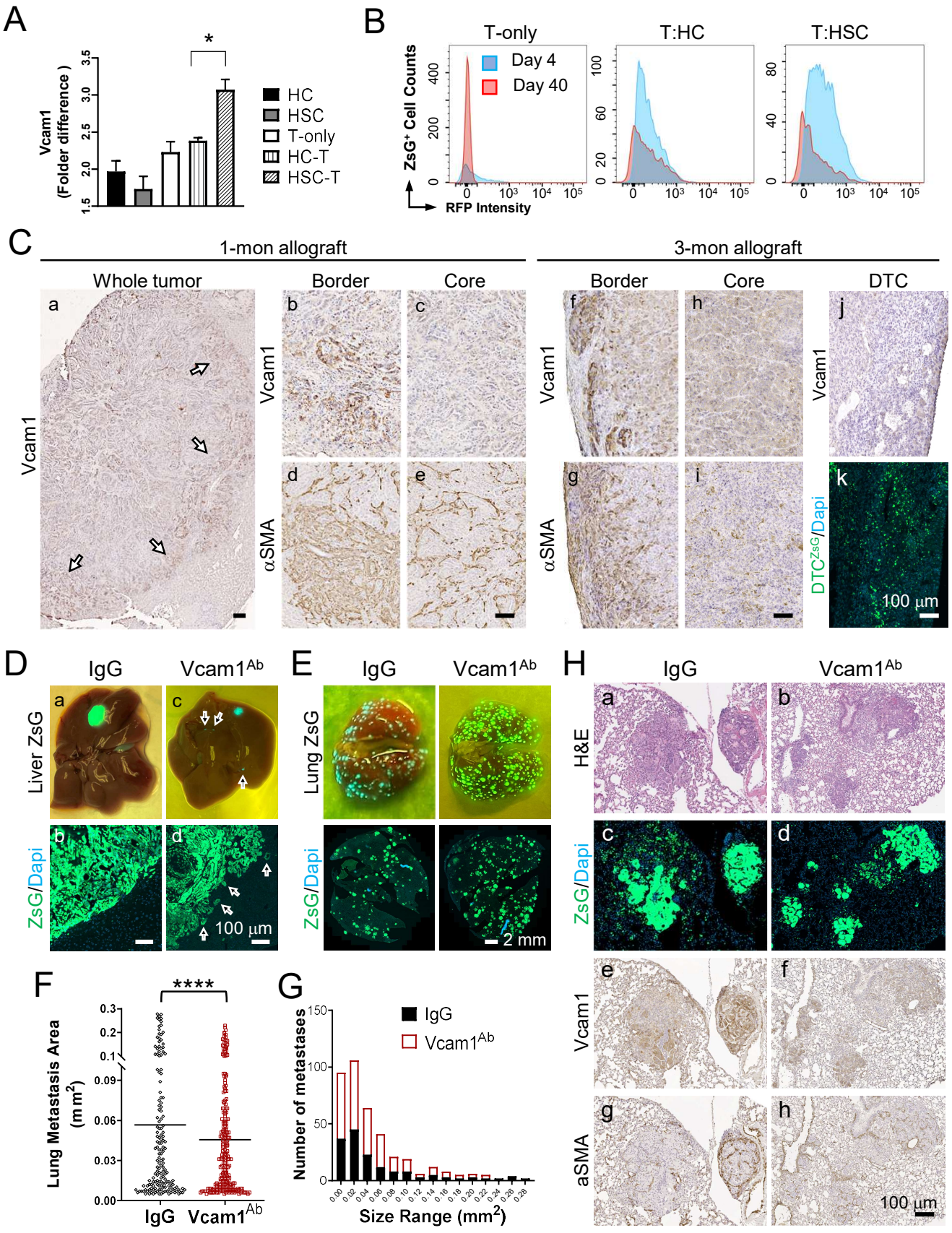

Figure 7